Energy Conversion and Management 125 (2016) 347–352

Contents lists available at ScienceDirect

Energy Conversion and Management

journal homepage: www.elsevier.com/locate/enconman

Electrochemical behavior of pitch-based activated carbon fibers for electrochemical capacitors

Hye-Min Lee [a,b], Lee-Ku Kwac [c], Kay-Hyeok An [a], Soo-Jin Park [b], Byung-Joo Kim [a,*]

[a] R&D Division, Korea Institute of Carbon Convergence Technology, Jeonju 561-844, Republic of Korea
[b] Department of Chemistry, Inha University, Incheon 402-751, Republic of Korea
[c] Department of Manufacturing Technology and Design Engineering, Jeonju University, Jeonju 560-759, Republic of Korea

ARTICLE INFO

Article history:
Available online 15 June 2016

Keywords:
Steam activation
Pitch
Activated carbon fiber
Electric double layer capacitors
Porous materials
Supercapacitor

ABSTRACT

In the present study, electrode materials for electrochemical capacitors were developed using pitch-based activated carbon fibers with steam activation. The surface and structural characteristics of activated carbon fibers were observed using scanning electron microscopy and X-ray diffraction, respectively. Pore characteristics were investigated using N_2/77 K adsorption isotherms. The activated carbon fibers were applied as electrodes for electrical double-layer capacitors and analyzed in relation to the activation time. The specific surface area and total pore volume of the activated carbon fibers were determined to be 1520–3230 m^2/g and 0.61–1.87 cm^3/g, respectively. In addition, when the electrochemical characteristics were analyzed, the specific capacitance was confirmed to have increased from 1.1 F/g to 22.5 F/g. From these results, it is clear that the pore characteristics of pitch-based activated carbon fibers changed considerably in relation to steam activation and charge/discharge cycle; therefore, it was possible to improve the electrochemical characteristics of the activated carbon fibers.

1. Introduction

Electric double-layer capacitors (EDLCs) have attracted considerable attention as efficient energy storage devices [1]. Their operation is based on charge accumulation at the electrode. EDLCs are very attractive as potential energy storage systems because of their high energy density (>10 kW/kg) [2], quick charge/discharge rate [1], and long, maintenance-free operation life (>10^6 cycles). Characteristics of supercapacitors make them a very suitable option for energy storage in both power applications [3] and electric vehicles [4].

Charge storage in EDLCs utilizes electrostatic adsorption of electrolyte ions at the electrode–electrolyte interface [5]. An ideal electrode material is expected to possess a high specific surface area [6], an optimal pore size distribution [7], electric stability, and electric conductivity for fast transport of the electrolyte ions and charges.

Porous carbonaceous materials with tunable porosities, including activated carbon (AC) [8], activated carbon fibers (ACFs) [9], ordered mesoporous carbons [10], carbon nanotubes (CNTs) [11], and graphene-based materials [12] have been used extensively as electrode materials in commercial EDLCs.

ACFs make up a porous carbon material that possesses unique electrochemical properties due to qualities such as a well-developed porous structure [9], high specific surface area, and high pore volume [13]. Pores of the ACF open directly to the outer surface, and the size of the pores falls within a narrow distribution.

Currently, research in supercapacitors is focused on increasing their energy densities further and lowering their overall production costs by finding suitable electrode materials [14]. Carbon nanotubes (CNTs) based electrodes were proposed to overcome the above limitation because of CNT's large electrical conductivity [15]. Despite this advantage, the use of CNTs in supercapacitors has been limited due to the presence of a high contact resistance between the supercapacitor electrode and current collector.

Pitch-based AC is expected to have a high carbon yield [9], a well-developed crystal structure [16], and superior electrical conductivity [17], compared to other forms of activated carbon. Furthermore, pitch-based high-crystallinity AC has the potential to be used as electrode material for EDLCs after an activation process to develop a porous structure [17]. Pitch-based ACFs exhibit high specific surface area showing adsorption/desorption with negligible hysteresis. Therefore, manufacture of EDLCs using ACF is expected to improve electrochemical stability [18].

Consequently, in the present study, steam was used to activate pitch-based ACFs to develop their pore structure. The textural properties of the well-developed ACF pores were investigated,

* Corresponding author.
E-mail address: kimbj2015@gmail.com (B.-J. Kim).

http://dx.doi.org/10.1016/j.enconman.2016.06.006
0196-8904/

including their specific surface area and pore structure. Also investigated were the electrochemical characteristics of electrodes fabricated with the ACF so produced, and of supercapacitors made of organic electrolytes. In this way, the effect of steam activation on the electrochemical characteristics of pitch-based ACF electrodes was determined.

2. Experiment details

2.1. Sample preparation

In the present study pitch-based CF (GS Caltex, Korea) was activated using steam. For the activation process, the temperature was elevated from room temperature (25 °C) to 900 °C at 10 °C/min in N_2 gas in a custom-made cylindrical steel tube (SiC heater; 1300 mm × 100 mm). The reactor tube was maintained in a steam atmosphere for either 10 min (ACF-10), 20 min (ACF-20), 30 min (ACF-30), or 40 min (ACF-40), and then cooled down once again to room temperature, still in N_2 gas.

2.2. Characterizations

The pore structure of the ACs was characterized by N_2 adsorption/desorption at 77 K using a BELSORP-max (BEL JAPAN, Japan). All ACFs were degassed at 300 °C for 6 h prior to measurement. The specific surface area was calculated within the relative pressure interval of 0.01–0.2 using the Brunauer-Emmett-Teller (BET) method [19]. Pore size distribution in the mesopore range was obtained by the Barrett-Joyner-Halenda (BJH) method [20]. The microstructure of the ACFs was determined using a wide-angle X-ray diffractometer (WAXRD), employing a Rigaku SmartLab X-ray diffractor with customized auto-mount and a Cu Kα radiation source. Diffraction patterns were collected within the diffraction angles from 5° to 90° with a speed of 2 °/min. The morphology of the ACFs was explored using a field emission scanning electron microscope (FE-SEM, S-4800, HITACHI, Japan). To reduce charging during FE-SEM imaging, the samples were first placed on a sample holder and coated with platinum.

2.3. Electrochemical measurements

The electrodes were prepared by coating aluminum foil with an aqueous ACF suspension (87 wt%) mixed with carboxy-methylcellulose binder (CMC, 4 wt%), a plasticizer (styrenebutyrene rubber (SBR), 3 wt%), and a conductive agent (carbon black, 10 wt%). A coin-type capacitor cell was used to examine the electrochemical performance of the ACF electrodes, which consisted of a carbon film (diameter 14 mm, ~200 μm thick) and Al foil as the current collector. This cell consisted of two, facing carbon electrodes, sandwiching a cellulose filter paper as the separator. All electrochemical measurements were carried out using organic electrolyte 1 M $(C_2H_5)_4NBF_4$/propylene carbonate at room temperature.

To verify the charge and discharge characteristics of the cells produced, a charge/discharge tester (Maccor 4300 k desktop; Maccor, USA) was used for charging and discharging via the galvanostatic method. Measurements were made at a driving voltage of 0.1–2.5 V, and a current density of 2 mA/cm^2, during charge and discharge. The produced cell was measured based on the capacitance per unit weight combining conductive material and binder (F/g). It is necessary to confirm definitely the electrode capacity evaluation method. This is due to the fact that many numbers quoted are not electrode mass and quite often relate only to the active material and do not include the mass of the binders, conductive carbon fillers. Again, this makes comparison of numbers in the literature often difficult.

The cyclic voltammetry (CV) and electrochemical impedance spectroscope (EIS) measures were collected using an electrochemical device (VSP; Biologic, USA). The CV was found to be 30 mV/s at 0.1–2.5 V, and the Nyquist plots were recorded potentiostatically (0 V) by applying an alternating voltage of 10 mV amplitude in the 10 MHz–300 kHz frequency range.

3. Results and discussion

3.1. Surface morphology analysis

Fig. 1 presents the FE-SEM images of the ACF, which were used to investigate the effects of steam activation on the surface morphology. All images were taken at a magnification of 10,000× or 200,000×. For the as-prepared CF and all ACF samples (Fig. 1a–i), the fiber shape was maintained despite the severe conditions of the activation process. The CFs (Fig. 1a) prepared through the melt-spinning process were round with a smooth surface. The pores that developed on the surface due to activation can be seen in Fig. 1c–j. The high-magnification images (Fig. 1f, h, and j) show that the number of pores increased with the time of steam activation. In addition, as the activation time increased, micropores developed into mesopores, which then collapsed and developed into macropores.

3.2. Adsorption isotherm and textural properties

Fig. 2 shows the typical N_2 adsorption/desorption isotherms for CFs and ACFs prepared in this work. The ACFs showed a mixture of IUPAC Type I and Type IV [21]. The data about N_2 adsorption at 77 K were listed in Table 1.

The specific surface area of the ACFs increased with increasing activation time. It is clear that the surface area and pore structure were significantly influenced by the activation time. The specific surface area and the pore volume of the as-received CF were about 5 m^2/g and 0 cm^3/g, respectively. However, the specific surface area of the ACFs varied between 1520 and 3230 m^2/g. It reached a maximum value of 3230 m^2/g at 40 min, indicating that continuous activation is beneficial for obtaining ACFs with the greatest specific surface area.

Based on the literature for pitch-based ACFs, it was expected that the specific surface area would increase with burn off. The specific surface area of ACF was increased by activation with a corresponding decrease in carbon yield. ACF-20 resulted in 1750 m^2/g specific surface area and 64% (w/w) yield (36% burnt off). The specific surface area and the carbon yield of ACF-30 changed remarkably (2650 m^2/g and 34%, respectively).

Fig. 3 shows the mesopore distribution of the prepared ACF, calculated using the BJH method. When the mesopore distribution curve according to the BJH equation was examined (Fig. 4), it was possible to obtain results identical to those in Table 1. All the ACFs had their highest intensity peak around 2.0 nm. The ACNF-45 sample showed better-developed mesopores than did other ACFs. This means that increasing activation time results in larger pore size. Clearly, steam activation played an effective role in the development of mesopores.

3.3. X-ray diffraction

The crystallography of ACF produced from carbon fiber using steam activation, was characterized by means of X-ray diffraction (XRD). This information, for the CF and ACF prepared during this work, is presented in Fig. 5 and Table 2. It is well known that the oxidation of carbonaceous materials has a higher probability of occurring in the amorphous region and graphite edges [22].

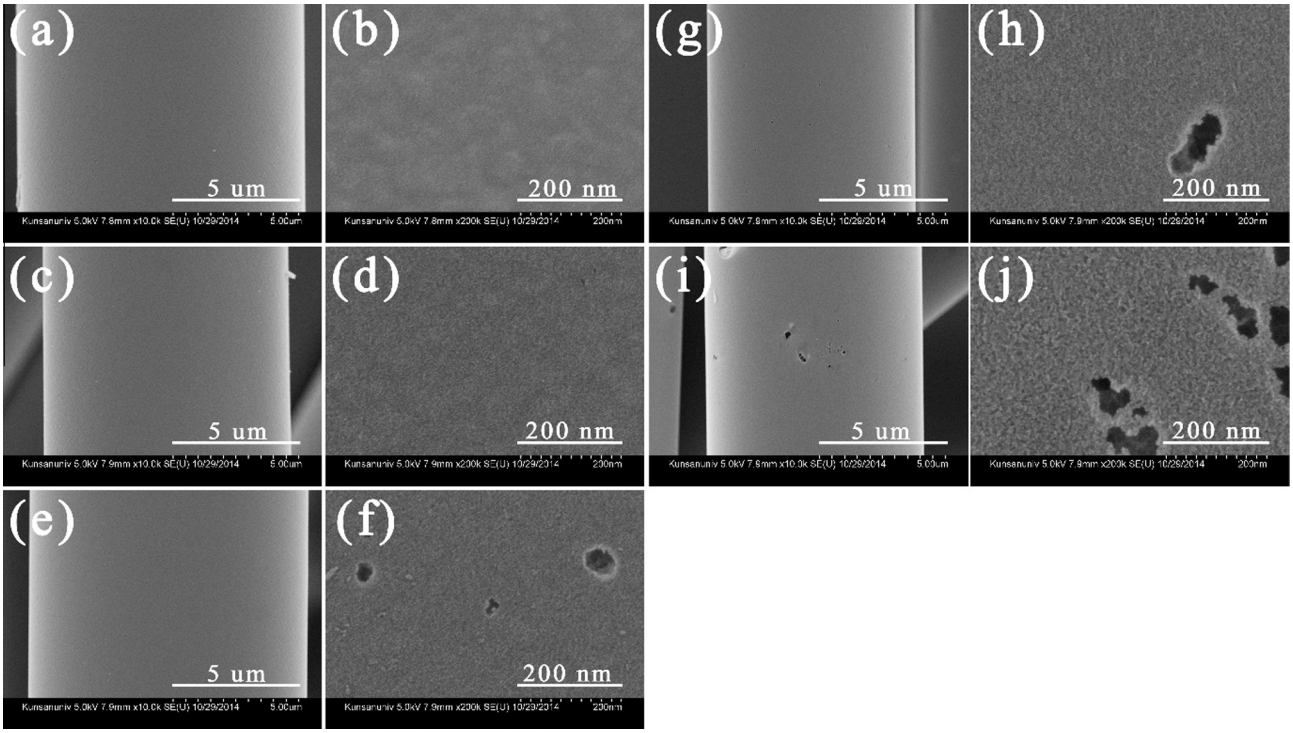

Fig. 1. SEM images of activated carbon fiber with different steam activation times: (a) As-received CF, (b) magnified image of (a), (c) ACF-10, (d) magnified image of (c), (e) ACF-20, (f) magnified image of (e), (g) ACF-30, (h) magnified image of (g), (i) ACF-40, (j) magnified image of (i).

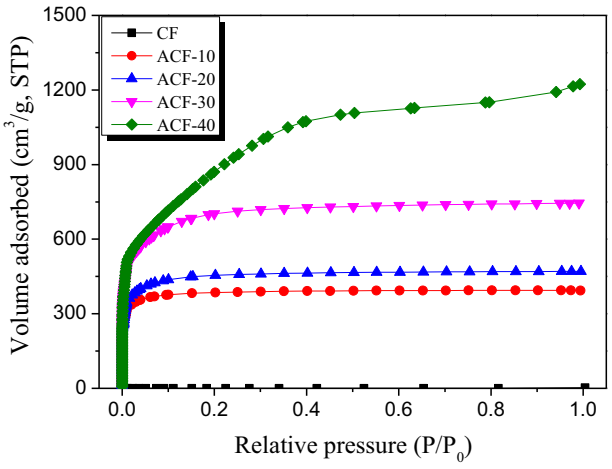

Fig. 2. N_2/77 K adsorption–desorption isotherm curves of activated carbon fiber with different steam activation times.

If carbon atoms in the amorphous region of CFs are removed first, the crystallinity of the remaining CF can be increased due to the reduction of a portion of the amorphous region. This results in the increased L_c or L_a of activated fibers. From this, there will be a significant change in d_{002} and an expected decrease of L_c or L_a, if carbon atoms on the graphite edges are removed after oxidation of the amorphous region. In fact, for the activation time of 10 min, L_c showed an increase, owing to the oxidation of amorphous carbon.

The next stage had activation times of 20, 30, or 40 min. The development of pore characteristics was accelerated in this stage, compared to other activation periods. The specific surface area surged from 1750 to 2650 to 3230 m^2/g, respectively, while the total pore volume increased from 0.73 to 1.15 to 1.89 cm^3/g. As the activation time increased to 40 min, L_c showed a continuous decrease, owing to the oxidation of carbon atoms at the graphite edges. Meanwhile, the oxidation of graphite edges throughout activation can be regarded as the cause of decreasing L_c.

3.4. Electrochemical characterizations

The electrochemical properties, including galvanostatic charge/discharge of the ACF electrodes, were studied using an electrolyte of 1 M $(C_2H_5)_4NBF_4$/propylene carbonate solution. Fig. 6 shows the change in the capacitance according to the charge/discharge cycle. The specific capacitances of all samples increased with increasing activation times in the first cycle. Normally, the specific

Table 1
Textural properties of activated carbon fiber with different activation methods.

Sample	Activation conditions	S_{BET} (m^2/g)	V_{Total} (cm^3/g)	V_{Meso} (cm^3/g)	V_{Micro} (cm^3/g)	C_g (F/g)	
						Cycle 1	Cycle 20
ACF	–	5	0	0	0	–	–
ACF-1	900 °C × 10 min	1520	0.61	0.03	0.58	1.1	21.6
ACF-2	900 °C × 20 min	1750	0.73	0.06	0.67	1.1	20.1
ACF-3	900 °C × 30 min	2650	1.15	0.17	0.98	15.8	16.9
ACF-4	900 °C × 40 min	3230	1.89	1.06	0.83	22.5	20.6

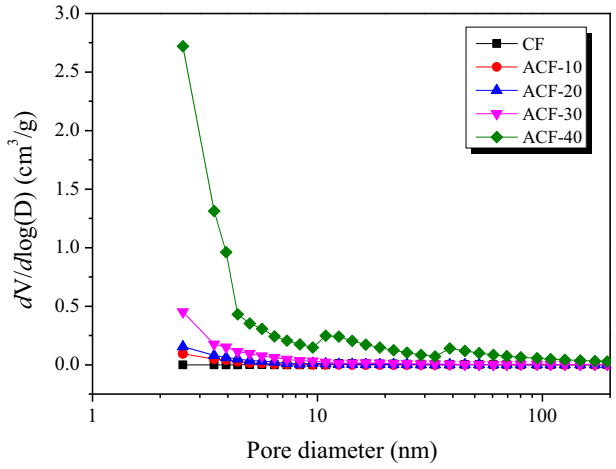

Fig. 3. Pore size distribution of activated carbon fiber with different steam activation times.

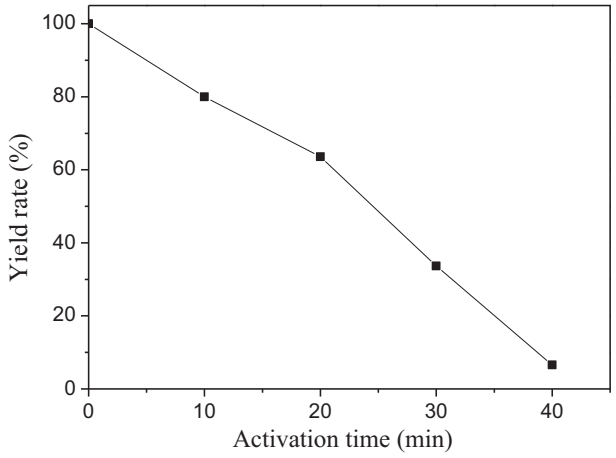

Fig. 4. Yield rate of activated carbon fibers with different steam activation times.

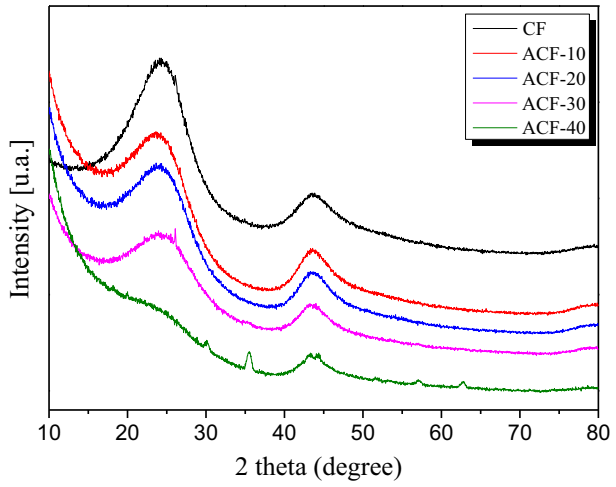

Fig. 5. X-ray diffraction patterns of activated carbon fiber with different steam activation times.

capacitance of ACF is strongly related to its mesoporosity [9]. In this work, ACF-40 showed the best mesoporosity and 22.5 F/g of energy storage ability in the first cycle. A unique trend in the

Table 2
Structural parameters of activated carbon fiber with different activation methods.

	002 peak				10*l* peak			
	2θ (°)	d_{002} (Å)	FWHM (2θ)	L_c (Å)	2θ (°)	d_{10l} (Å)	FWHM (2θ)	L_a (Å)
ACF	24.08	3.69	7.99	10.18	44.00	2.06	5.65	31.03
ACF-10	24.12	3.69	7.19	11.31	43.86	2.06	5.51	31.80
ACF-20	24.37	3.65	7.28	11.17	43.78	2.07	5.64	31.06
ACF-30	24.69	3.60	7.80	10.44	43.85	2.06	5.61	31.24
ACF-40	24.13	3.69	8.50	9.57	43.86	2.06	5.62	31.18

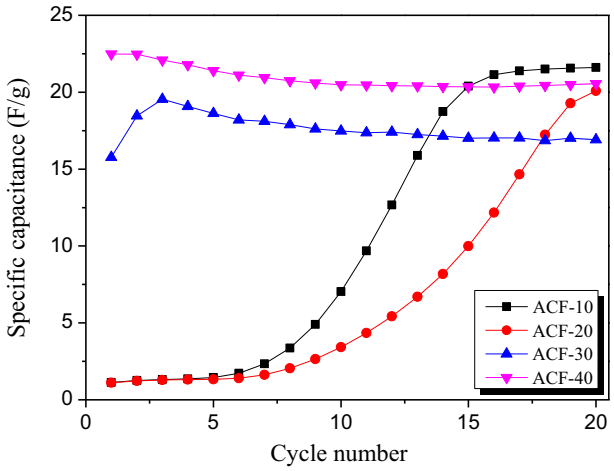

Fig. 6. Variations of specific capacitance in relation to cycle number.

charge/discharge curve was observed for ACF-10 and ACF-20 with increasing number of cycles. The specific capacitance of ACF-10 and ACF-20 increased after the fifth cycle, and was higher than that of ACF-30 and ACF-40.

Generally, the reason for the increased specific capacitance is increased wetting of the electrode with the electrolyte as the number of charge/discharge cycles increases. However, this provided a very small increase, which was also observed in Cycles 1–3 of ACF-30.

Honma et al. [23] reported increased capacitance related to intercalation of ions between graphene layers, due to expansion of interlayer distance. In this work, the increase in the specific capacitance of ACF-10 and ACF-20 was determined by changed pore structure during charging and discharging. After Cycle 20, a specific capacitance of 21.6 F/g was achieved, though the mesopore volume was only 0.03 cm^3/g. The capacitance per unit weight of electrode (active material, binders, and conductive carbon fillers) was measured and it was compared with YP-50F (YP-50F is the most widely used activated carbon for EDLC.) from Kuraray Chemical Corporation. The specific capacitance of ACFs were over 21.6 F/g (capacitance per unit weight of electrode, full-cell) and they were higher than of YP-50F (19 F/g, capacitance per unit weight of electrode, full-cell) [24]. These results suggest that the pore structure of the pitch-based activated carbon fibers induced higher capacitance.

Fig. 7 shows typical galvanostatic charge/discharge curves of the ACF electrode at various current densities, and change of the specific capacitance in relation to current density, for all samples. The specific capacitance increased with increasing specific surface area in Cycle 1. By contrast, the specific capacitance of ACF-10 and ACF-20 increased with increasing discharge time, as indicated in the charge/discharge curves. For ACF-30, the charging time was the same for Cycle 1 and Cycle 20, but the increasing discharge

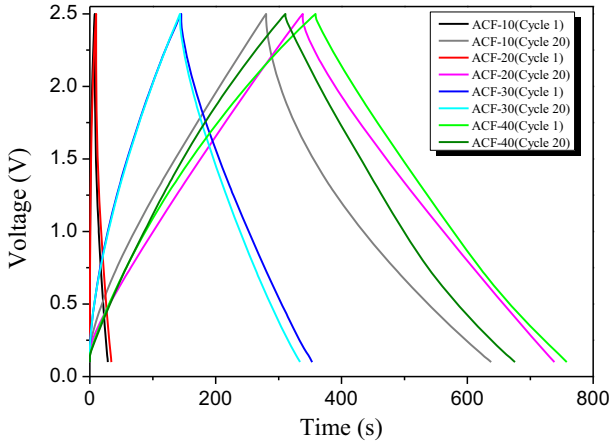

Fig. 7. Charge-discharge curves of activated carbon fiber as a Cycle 1 - Cycle 20.

time was determined by wetting of the electrode, with a related increase in specific capacitance.

Fig. 8 shows the results of cyclic voltammograms (CV) measured at a scanning rate of 30 mV/s, within the voltage range of 0–2.5 V, using electrodes of the produced ACF. As activation time increased, the area of the CVs tended to increase. The CV curves of all the ACFs were distinguished by specific capacitance at Cycle 1 (first cycle). However, as Fig. 8b shows, the CVs of all ACFs took on a square shape characteristic of EDLCs, at Cycle 20. Moreover, the ACFs showed a symmetric, quasi-rectangular shape profile typical of ideal EDLCs. Overall, with increasing activation time, the CV area remained fixed. Wetting of the electrode with the electrolyte solution was confirmed as causing the ACR-30 curve to change from oval to rectangular.

Fig. 9 shows the complex impedance spectra of various samples. The frequency was swept from 10 MHz to 300 kHz. As activation time and number of cycles increased, the impedance curves tended not to change. However, after Cycle 20, the CV curve changed with increasing activation time. The ideally polarizable capacitance should give rise to a straight line along an imaginary axis. In a real capacitor with series resistance, this line has a finite slope, representing the diffusive resistivity of the electrolyte within the pores of the electrode. It was found that the diffusive line of the ACF electrode came closer to an ideally straight line with increased activation time.

An increase in activation time from 0 to 40 min reduced the resistance of the sample. The formation of abundant micropores and mesopores may also enhance the diffusivity of the hydrated ions in the pores and consequently reduce the resistance of the ACF electrode. In addition, change related to increased number of cycles was most significant in ACF-20 and ACF-30.

Pore shapes affect impedance behavior, specifically, the form of the impedance [25]. The pores of ACF-20 were initially cylindrical or wedge-shaped. However, semi-circular pores were observed by

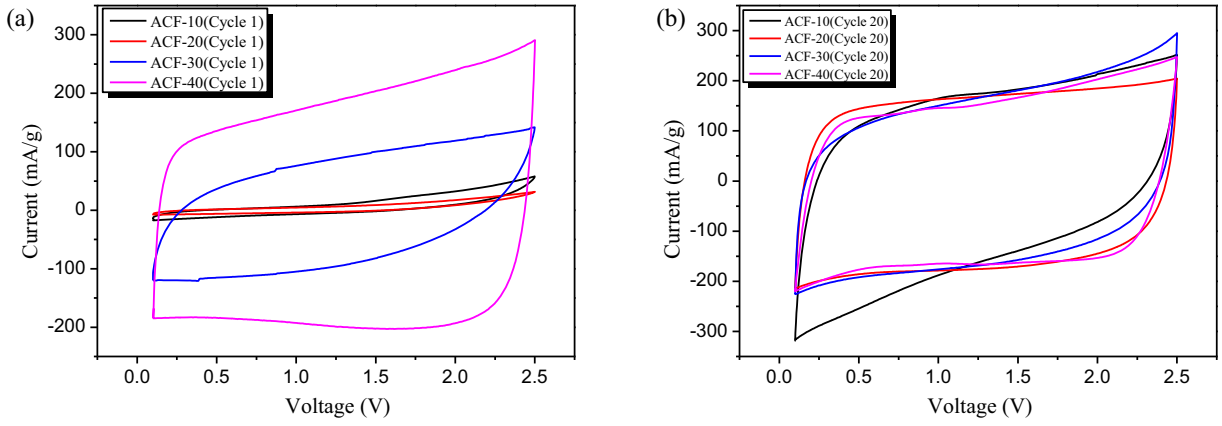

Fig. 8. Cyclic voltammograms of activated carbon fiber with different steam activation times: (a) Cycle 1 and (b) Cycle 20.

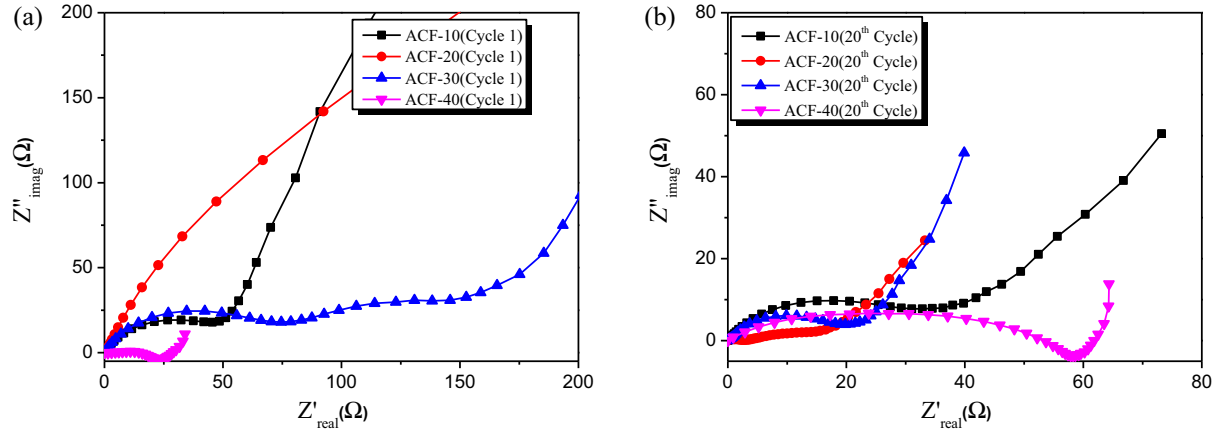

Fig. 9. Nyquist plot of activated carbon fiber with different steam activation times; (a) Cycle 1 and (b) Cycle 20.

Cycle 20. The increased capacity of ACF-30 was determined to be due to reduction in the size of the semi-circular pores due to wetting of the electrode.

4. Conclusion

In this work, pitch-based ACFs were prepared using different activation times in order to produce high specific-surface-area and mesopore-rich pore-structure. Specific surface area was increased with increasing activation time and burn off. The specific surface area surged from 1750 to 2650 to 3230 m^2/g, respectively. High mesopore volume ACFs (up to 1.06 cm^3/g) with specific surface area as large as 3230 m^2/g can be prepared from a pitch-based CF. Increased activation time induced higher specific surface area and larger pore size, which resulted in higher capacitance and better rate capability at Cycle 1. ACF-40 showed the best mesoporosity and 22.5 F/g of energy storage ability in the first cycle. Specific capacitance was changed by increasing charge/discharge cycle. For ACF-30, the specific capacitance was the same for Cycle 1 and Cycle 20, but the increasing specific capacitance was determined by wetting of the electrode. And ACF-40 was observed in stable cycle life. However, the specific capacitance of ACF-10 and ACF-20 continued to increase per cycle until Cycle 20. The ACF-10 sample showed the best specific capacitance. It was determined that the pores were expanded by moving ion during the charge/discharge cycles. Based on the charge-discharge characteristics, ACF-10 showed the best result (21.6 F/g and 20% burn off) of all the ACF samples at Cycle 20.

Acknowledgments

This study was supported by a grant from the "Carbon Valley R&D Project (Project no. R0002651), Material & Component Technology Development Project (Project no. 10050391), and National Research Foundation of Korea (Project no.2014R1A2A1 A11053533)", funded by the Ministry of Trade, Industry & Energy (MOTIE) and Korea government (MSIP), Republic of Korea.

References

[1] Sharma P, Bhatti TS. A review on electrochemical double-layer capacitors. Energy Convers Manage 2010;51:2901–12.
[2] Conway BE. Transition from 'Supercapacitor' to 'Battery' behavior in electrochemical energy storage. J Electrochem Soc 1991;138:1539–47.
[3] Kyriakarakos G, Piromails DD, Arbanitis KG, Dounis AI, Papadakis G. On battery-less autonomous polygeneration microgrids: investigation of the combined hybrid capacitors/hydrogen alternative. Energy Convers Manage 2015;91:405–15.
[4] Teymourfar R, Asaei B, Iman-Eini H, Nejati fard R. Stationary super-capacitor energy storage system to save regenerative braking energy in a metro line. Energy Convers Manage 2012;56:206–14.
[5] Yoshida A, Tanahashi I, Nishino A. Effect of concentration of surface acidic functional groups on electric double-layer properties of activated carbon fibers. Carbon 1990;25:611–5.
[6] Hui TS, Zaini MAA. Potassium hydroxide activation of activated carbon: a commentary. Carbon Lett 2015;16:275–80.
[7] Zhang L, Yang X, Zhang F, Long G, Zhang T, Leng K, et al. Controlling the effective surface area and pore size distribution of sp^2 carbon materials and their impact on the capacitance performance of these materials. J Am Chem Soc 2013;135:5921–9.
[8] Lee EJ, Kwon SH, Choi PR, Jung JC, Kim MS. Activated carbons prepared from mixtures of coal tar pitch and petroleum pitch and their electrochemical performance as electrode materials for electric double-layer. Carbon Lett 2015;16:78–85.
[9] Diez N, Díaz P, Álvarez P, González Z, Granda M, Blanco C, et al. Activated carbon fibers prepared directly from stabilized fibers for use as electrodes in supercapacitors. Mater Lett 2014;136:214–7.
[10] Mitome T, Uchida Y, Egashira Y, Nishiyama N. Synthesis of ordered mesoporous carbon films with a 3D pore structure and the electrochemical performance of electrochemical double layer capacitors. Colloids Surfaces A: Physicochem Eng Aspects 2014;449:51–6.
[11] Wen S, Jung M, Joo OS, Mho SI. EDLC characteristics with high specific capacitance of the CNT electrodes grown on nanoporous alumina templates. Curr Appl Phys 2012;6:1012–5.
[12] Zhang T, Zhang F, Zhang L, Lu Y, Zhang Y, Yang X, et al. High energy density Li-ion capacitor assembled with all graphene-based electrodes. Carbon 2015;92:106–18.
[13] Lee HM, Kim HG, An KH, Kim BJ. Effects of pore structures on electrochemical behaviors of polyacrylonitrile-based activated carbon nanofibers by carbon dioxide activation. Carbon Lett 2014;15:71–6.
[14] Gund GS, Dubal DP, Chodankar NR, Cho JY, Gomez-Romero P, Park C, et al. Low-cost flexible supercapacitors with high-energy density based on nanostructured MnO_2 and Fe_2O_3 thin films directly fabricated onto. Sci Rep 2015;5:12454.
[15] An KH, Kim WS, Park YS, Moon JM, Bae DJ, Lim SC, et al. Electrochemical properties of high-power supercapacitors. Adv Funct Mater 2001;11:387–92.
[16] Guo Y, Shi ZQ, Chen MM, Wang CY. Hierarchical porous carbon derived from sulfonated pitch for electrical double layer capacitors. J Power Sour 2014;252:235–43.
[17] Torchała K, Kierzek K, Gryglewicz G, Machnikowski J. Narrow-porous pitch-based carbon fibers of superior capacitance properties in aqueous electrolytes. Electrochim Acta 2015;167:348–56.
[18] Tomko T, Rajagopalan R, Lanagan M, Foley HC. High energy density capacitor using coal tar pitch derived nanoporous carbon/MnO_2 electrodes in aqueous electrolytes. J Power Sour 2011;196:2380–6.
[19] Brunauer S, Emmet PH, Teller WE. Adsorption of gases in multimolecular layers. J Am Chem Soc 1938;60:309–19.
[20] Barrett EP, Joyner LG, Halenda PP. The determination of pore volume and area distributions in porous substances. I. Computations from nitrogen isotherms. J Am Chem Soc 1951;73:373–80.
[21] Sing KSW, Everett DH, Haul RAW, Moscou L, Pierotto RA, Rouquerol J. Reporting physisorption data for gas/solid systems with special reference to the determination of surface area and porosity. Pure Appl Chem 1985;57:603–19.
[22] Sharma A, Kyotani T, Tomita A. A new quantitative approach for microstructural analysis of coal char using HRTEM images. Fuel 1999;78:1203–12.
[23] Mitani S, Sathish M, Rangappa D, Unemoto A, Tomai T, Honma I. Nanofraphene derived from carbon nanofiber and its application to electric double-layer capacitors. Electrochim Acta 2012;68:146–52.
[24] Kim JA, Park IS, Seo JH, Lee JJ. A development of high power activated carbon using the KOH activation of soft carbon series cokes. Teans Electr Electron Mater 2014;15:81–6.
[25] Kaiser H, Beccu KD, Gujahr MA. Abschätzung der porenstruktur poröser elektroden aus impedanzmessungen. Electrochem Acta 1976;21:539–43.